AIMS Geosciences

AIMS Geosciences, 7(2): 162–179.
DOI: 10.3934/geosci.2021010
Received: 30 November 2020
Accepted: 29 March 2021
Published: 08 April 2021

http://www.aimspress.com/journal/geosciences

Research article

Assessment of health status of tree trunks using ground penetrating radar tomography

Maria Sudakova[1,2,*], Evgeniya Terentyeva[1] and Alexey Kalashnikov[3]

[1] MSU Lomonosov, geology faculty, seismic department, 119991, GSP-1, 1 Leninskiye Gory, Moscow, Russia
[2] Earth Cryosphere Institute Tyumen Scientific Centre SB RAS, 625000, Maligyna, 86, Tyumen, Russia
[3] Moscow State University of Civil Engineering, 129337, 26, Yaroslavskoye Shosse, Moscow Russia

* **Correspondence:** Email: m.s.sudakova@yandex.ru; Tel: 79104809299.

Abstract: Typical tree health assessment methods are destructive. Non-destructive Ground Penetrating Radar (GPR) technique can provide a diagnostic tool for assessing the health status of live tree trunks based on internal dielectric permittivity distribution. Typical GPR acquisition technique—common-offset—is not helpful in providing robust and high-resolution quantitative results. In the current work we evaluate the capabilities of GPR tomography on locating tree-decays in a number of different tree species, imaging the interval structure of a healthy tree and quantitative estimation of moisture content (MC) based on distribution of dielectric permittivity, directly related to MC. The measurements described in this work were made on the trunks of live trees of different species in different conditions: a "healthy" English oak (Quercus robur), a "dry" Siberian fir (Picea obovata), a Horse chestnut (Castanea dentata) and a European aspen (Populus tremula) with rot inside. The results of the suggested approach were confirmed by resistography. Different parts of the trunk (bark, core, sapwood), as well as healthy and affected areas differ in moisture content, so the method of GPR tomography allowed us to see both the structure of the trunk of a healthy tree, and the presence and dimensions of defects.

Keywords: non-destructive testing; tree stability; wood decay; wood moisture content; trees monitoring

1. Introduction

Tree health assessment is used to preserve and maintain historical park ensembles, and for the safety of the urban environment. The impact of negative factors such as stress or illness can lead to changes in the physical characteristics of trees, and in rare cases—to the loss of a tree. Recently, in addition to visual inspection, which may not reveal internal damage, instrumental methods became popular, both destructive, with a probe/penetrometer [1], and non-destructive, such as electric tomography and acoustic methods, including ultrasound and acoustic tomography [2–5].

The assessment of tree health requires visual assessment, and investigations of the internal structure. Visual assessment includes both inspection of visible internal defects [6], as well as instrumental measurements of defects and assessment of wood strength [7,8]. Instrumental assessment includes both direct and indirect research methods. Among those are: resistography method, when resistance to drilling is read by the device and converted into a resistogram, which indicates the density of wood [9], electric tomography [4], acoustic tomography [3] etc.

The electric tomography method provides an image of the resistivity distribution in the section of a live tree. Variations in resistivity values may indicate rotting processes or differences in the properties of different sections of wood within a living tree [10]. The main drawback of this method is low conductivity of the tree bark, and, as a result, unreliable voltage measurement.

Acoustic tomography is another method that can be used to produce an image of the internal structure of a tree by recording the propagation speed of a sound wave. Past research [11] presents the possibilities of the acoustic tomography in relation to the problems of numerical evaluation of rotting volumes in the trunks of living trees. The accuracy of the result is affected both by the contact of the sensors with bark and signal attenuation, in some cases it is necessary to introduce the sensors under the bark.

Despite the informative nature of these methods in wood diagnostics, they have significant disadvantages that prevent from being used widely: they are based on drilling, and can lead to a death of a tree, since fungal spores can penetrate into the hole [12]. Electric tomography [4] is carried out via electrodes placement into the tree to a depth of about 3 or 4 cm, and the resistograph requires drilling and penetrates to a depth of 150 mm. Even acoustic tomography [3] carries some risks, since during operation, nails are driven into the bark of a tree to install sensors. In addition, acoustic waves treat voids as low-velocity anomalies. Therefore ray coverage in voids will be low, which leads to incorrect estimation of velocity and anomaly dimension. The external bark of the tree may be damaged during the measurements, which can negatively affect tree viability. Moreover, the acoustic measurements are characterized by low resolution due to the wavelength range.

Ground penetrating radar (GPR) method has already become a widely successful method for solving many engineering problems. The scope of GPR studies is steadily expanding, and progress has been made in detection and 3D mapping of tree roots, assessment of their biomass [13–15], assessment of damage to the basements of constructions caused by tree roots [16], etc. The use of GPR in detecting rot in tree trunks is discussed in [17,5]. GPR wood investigations include the study of defects in timber bridge girders [18,19], wooden logs [20], historic timber beam [21], investigation of dielectric properties, anisotropy, and moisture in pine species [22]. However some papers [23] focus on difficulties when using GPR in combined source and receiver mode which results in poor contact of antennas with bark, difficulties in data interpretation [24], and high frequencies attenuation (1000 MHz). The tomographic approach in GPR was previously used to determine the location of the root system [13].

In this paper, we discuss the GPR tomography method, which was rarely applied to live trees. GPR tomography has been successfully used to search for voids in engineering structures [25]. The result of GPR tomography is quantitative as opposed to GPR in combined Source-Receiver mode (common-offset method). The method involves recalculation of direct wave travel-times into velocity values, and then into dielectric permittivity.

The measurements described further, were made on the trunks of live trees of different species in different conditions: a "healthy" English oak (Quercus robur), a "dry" Siberian fir (Picea obovata), a Horse chestnut (Castanea dentata) with rot inside, and European aspen (Populus tremula) with rot inside either. The result of GPR tomography represents high resolution distribution of dielectric permittivity inside the trunk. Based on correlation relationships, we determined the distribution of moisture content inside the trunk, and estimated rotten area in horse chestnut (Castanea dentata) and European Aspen (Populus tremula). The result of GPR tomography investigation of European Aspen (Populus tremula) was confirmed by resistograph measurements.

2. Materials and methods

2.1. Trees

The experiments were carried out in an urban environment on different trees species in different health condition (after visual inspection). All measurements were carried out during a day time. The photos of tree are provided in Figure 1.

2.1.1. English oak (Figure 1A)

Visual inspection demonstrates that the oak was healthy. There were no external defects of the trunk. There were no dry branches or dry leaves. The leaves were green without discoloration. Oak bark was uniform. The height of the tree is about 7 m, the trunk circumference at 140 cm from the ground is about 280 cm.

2.1.2. Fir (Figure 1B: the leftmost tree)

The height of the tree is about 12 m, the circumference at 140 cm from the ground is about 165 cm. The tree was visually "dry": about half of the branches with dried needles were orange, but without trunk defects. The bark was uniform.

2.1.3. European aspen (Figure 1C)

Visually it is also a healthy tree, the height of the tree is about 10 m. Circumference at 140 cm from the ground is 178 cm. Photo of the European Aspen is shown in Figure 1C. Red colour indicates the receiving antenna movement around the trunk. The photo shows a resistograph next to the tree.

2.1.4. Horse chestnut (Figure 1D)

The chestnut is about 10 m high, the trunk circumference at a height of 140 cm from the ground is about 195 cm. The tree has internal trunk defects: a hole filled with humus is observed inside the tree. The hole can be seen visually at a height of about 2 m, the hole depth is more than 1 m. However, the tree is alive visually: there are no signs of disease, no dry branches and leaves, leaves colour is uniform. In the photo, next to the chestnut tree there are the antennas that were used in the study. The yellow line is the tape measure.

Figure 1. Photos of the trees under study: a "healthy" English oak (Quercus robur) —A; a "dry" Siberian fir (Picea obovata) —B; the leftmost, European Aspen (Populus tremula) —C with rot inside and a horse chestnut (Castanea dentata) with rot inside either—D.

2.2. GPR tomography

2.2.1. Data acquisition and processing

The GPR survey was carried out at a height of 140 cm from the ground surface for all the trees except the horse chestnut. To explore the variation of internal defect in the chestnut trunk, measurements were taken at two heights: 150 cm and 95 cm.

GPR Zond-12e was used in data acquisition. Shielded bowtie antennas with a central frequency in the air of 2000 MHz were used as sources and receivers. The acquisition geometry layout is shown at Figure 2A. The measurement points were located in a horizontal plane along the perimeter of trunks. The transmitting antenna (source) was placed manually by one person at the first transmitting point against the trunk of a tree and the receiver was moved manually by another person along the circumferential receiving line to acquire a complete radargram at the selected trunk level. At the next step, the source is relocated by 10 cm from the second transmitting point and the receiver is moved along the circumferential line to acquire the second radargram. The cycle is repeated at every transmitting point around the trunk. It required two people and about half an hour to acquire the data for one slice. To eliminate the nonwave component of electromagnetic field, the minimum distance between the transmitting and the receiving antennas was 20 cm. The antenna orientation on the profile was co-polarized broadside. The work was carried out in continuous mode and field trace spacing was about 1 mm. To reduce the time spent during processing, the trace spacing was increased to 1 cm. The traces positioning was performed using a tape measure and markers placed in 10 cm increments.

Figure 2B demonstrates the forward problem solution: traveltime curves, predicted in isotropic tree trunk (at constant velocity). The first arrival corresponds to air wave travelling at velocity 30 cm/ns. The traveltime curve is a straight line. The second arrival corresponds to direct signal travelling through the trunk. The traveltime curve is hyperbolic in isotropic case. The transmitter is stationary, the receiver is moved along the circumferential receiver line. The arrival time increases with transmitter-receiver offset, achieves maximum (when transmitter-receiver are located on opposite sides of a trunk, with offset equal to the diameter) and decreases as the receiver approaches the transmitter.

As a result, for each "slice" of the trunks several thousands of traveltime samples were acquired. Data processing involved geometry update, trace number reduction, and delay removal based on air wave arrival time. After processing, the direct wave arrival time was determined. The picking was performed on a maximum phase, and then shifted to the first break time. The traveltimes were used to solve the inverse problem of ray tomography. The tree trunk was approximated by cylinder shape (the tree trunk was assumed to be perfectly cylindrical). Calculations were produced in GeoTomCG® software, the grid cell size was 2 by 2 cm.

Velocity values V in cm/ns were converted into the real part of complex dielectric permittivity ε according to the ratio:

$$\varepsilon = \left(\frac{30}{V}\right)^2 \tag{1}$$

The representation of the result in the form of the permittivity distribution is more obvious, since its value is directly related to the volume moisture (there are several works that describe this approach, for example [26,27]).

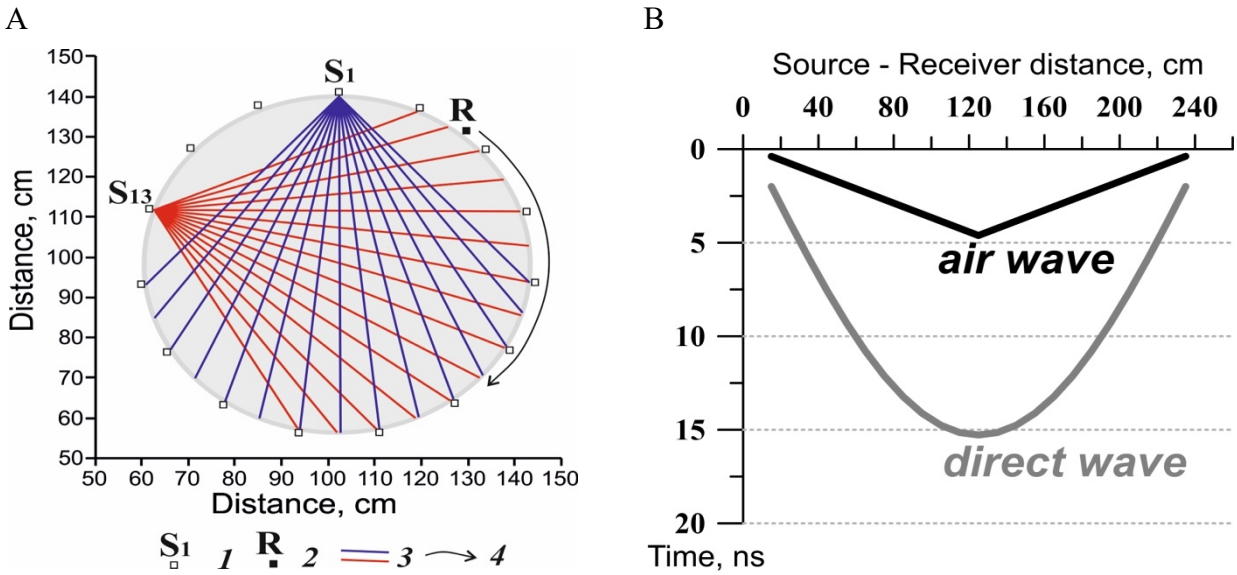

Figure 2. A—Acquisition geometry layout [1: source point; 2: moving receiver; 3: direct wave path (source number 1 and 13) and 4: receiver movement direction]; B—forward modelling.

2.2.2. Moisture content calculation

Moisture content (MC) affects many properties of the wood itself and the tree live condition. Moreover, high moisture may be associated with the risk of bio-deterioration—insect infestation or fungi growth. Moisture value in live trees is time-variant (different seasons) and depends on layers of the timber. Tree trunk moisture is always seeking equilibrium with the relative humidity of the air. As the air humidity varies over time—so does the moisture in the tree trunk.

Moisture content in wood is water to wood material ratio. The formula defines moisture as the weight of water in wood expressed as a percentage of oven-dry material weight:

$$MC = \frac{Wtest - Wovendry}{Woverdry} * 100\ \% \quad (2)$$

Wtest: weight of test wood; *Wovendry*: weight of oven-dry wood.

According to Equation (2), MC may range from 0% for oven-dry wood to over 100% when the water in the wood weighs more than the wood substance. The maximum MC depends of tree species and may achieve 140–150% [28]. The only direct method to determine MC in wood material is to measure the water content in a wood sample and the weight of oven-dry sample.

Laboratory electrophysical properties measurements on wood samples at different frequencies [29,30] showed that water is the main component that determines the electrophysical properties of wood, including the dielectric permittivity. The distribution of dielectric permittivity values inside the trunk directly indicates the distribution of moisture. A higher water content in wood results in increase in dielectric permittivity and consequently decrease in velocity of electromagnetic waves. Sbartaï et al. [31] have conducted sensitivity studies of radar signals to moisture variation in wood material. The measurements were carried out using 1.5 GHz antenna on 3 wood samples (Spruce, Pine, and Spruce glue-laminated timber). The results confirmed the effect of water and fibre direction on the dielectric permittivity of wood.

In our work, to estimate the moisture content in trees, correlation relationship between the real part of the dielectric permittivity versus moisture content were constructed. The calculation method we used is approximative, as it is based on assumptions and rounding. The measured values for the correlations were taken from [29]. In this book, the measured dielectric permittivity values versus measured moisture content are given for wood for different densities, at different temperatures and frequencies. The dielectric permittivity values are given only for 6 values of moisture content (0, 10, 20, 30, 60, 100%). In addition, average density values for different tree species growing on different continents are given in the work [29].

All our measurements were performed in Moscow in summer in sunny, moderately hot weather, with average temperature 20°C. The following density values were used: English Oak (Quercus robur) −0.68 g/cm^3, Siberian Fir (A. sibirica) −0.36 g/cm^3, American Chestnut (Castanea dentata) −0.47, European Aspen (Populus tremula) −0.46 g/cm^3. All density values were rounded to tenths. Torgovnikov [29] considered only two frequencies from GPR range: 100 MHz and 1 GHz, and relevant parameters for those. We estimated the dielectric permittivity value at 500 MHz as it corresponds to the dominant frequency of the direct wave signal determined experimentally during our observations.

It is generally assumed that in the GPR frequency range the real part of complex dielectric permittivity (ε') does not depend on the frequency [29,31]. However, some studies have reported that the ε' of wood decreases with frequency as much as 0–40% (at microwave frequencies) depending on the humidity and type of wood [33–35]. Based on these results, we applied logarithmic approximation to collate moisture content and dielectric permittivity at 500 MHz.

Dielectric permittivity, measured at frequency 10^8 and 10^9 Hz on wood samples with different density and moisture content modified from [29], are given in table 1. Also, the table shows values calculated at 500 MHz using logarithmic regression.

Table 1. Measured ε (adopted from [29]) and calculated pertmittivity for frequency 500 MHz (ε_{500}).

Frequency, Hz	MC (%)	Density 0.4 g/cm^3		Density 0.5 g/cm^3		Density 0.7 g/cm^3	
		ε	ε_{500}	ε	ε_{500}	ε	ε_{500}
10^8	0	1.7	1.7	1.9	1.8	2.3	2.2
10^9	0	1.7		1.8		2.2	
10^8	10	2.5	2.3	2.9	2.6	3.6	3.2
10^9	10	2.2		2.5		3.0	
10^8	20	3.5	3.1	4.1	3.6	5.3	4.7
10^9	20	2.9		3.4		4.4	
10^8	30	4.3	4.0	5.1	4.8	6.7	6.3
10^9	30	3.9		4.7		6.1	
10^8	60	7.4	6.1	10.1	7.9	13.9	10.8
10^9	60	5.6		6.9		9.4	
10^8	100	16.0	12.2	19.0	14.9	26.0	20.5
10^9	100	10.5		13.1		18.1	

The dielectric permittivity versus moisture content for various substances and media, including wood [27, 33, 36–38] at GPR frequencies can be expressed as follows:

$$\varepsilon = aW^3 + bW^2 + cW + d \quad (3)$$

a, b, c, d: are coefficients selected individually in each case.

Three correlation relationships were constructed for 20°C, the frequency of 500 MHz, and densities 0.4, 0.5, and 0.7 using the least squares method. In all cases, coefficient of determination or R2 was greater than 0.999. The calculated values of dielectric permittivity/moisture content are close to those cited in other papers [33,35].

2.3. Penetrometer

The penetrometer test was applied in this work because, until now, it is a standard method used in the "non-destructive testing" of trees (for example, [39]). One test was carried out by the Resistograph® 4 series at the investigated section of European Aspen. This test was made to verify the results of GPR, but without destroying the tree. Drilling with a resistograph was performed directly after GPR tomography. The drilling point was selected so that the profile was in the same plane as the GPR result (Figure 1C, red line). Figure 5C shows the drill profile overlaid on the GPR tomography to facilitate the comparison between the techniques.

3. Results

The results of observations are presented in the following order: live oak, dry fir tree, aspen (comparison with resistograph measurements), and chestnut with two sections. This order is chosen based on the following considerations: first we consider the distribution of dielectric permittivity and moisture in a live, healthy trunk, paying attention to isolines pattern and moisture values. Then we continue with a dry fir tree, then a section of aspen with rot inside, assessed by a penetrometer measurements. And in the end, we will consider the distribution of moisture in two different sections of chestnut.

Figures 3A, 4A, 5A, 6A demonstrate the examples of data acquired on different trees. The data is shown in variable density mode. The examples of two traces are also given: the first one obtained at the minimum source-receiver offset, and the second obtained at one of the maximum offsets when the source and receiver are on different sides of the trunk.

Two arrivals are highlighted in colour on radargrams: the air wave (first arrival) at velocity of 30 cm/ns is shown in purple, and the direct (target wave) is shown in white. Direct arrival propagating inside the trunk can be easily distinguished from air waves by its apparent velocity and apparent frequency, which are lower than that of air waves.

3.1. English oak (Quércus róbur)

A three-phase wavelet corresponds to direct arrival, with high amplitude against the background of noise (Figure 3A). Besides direct and air wave we can also pick other events corresponding to refracted multiples from the boundaries inside the trunk. The dielectric permittivity distribution reflects the concentric structure of the trunk of a living tree (Figure 3B). Various layers of the trunk can be distinguished inside: the core, sapwood, cambium, and bark. There are no abnormal zones, in terms of

structure and dielectric permittivity and moisture content values. The average dielectric permittivity is 18 with standard deviation 8.5%, the range of dielectric permittivity variation is from 14 to 44.

A

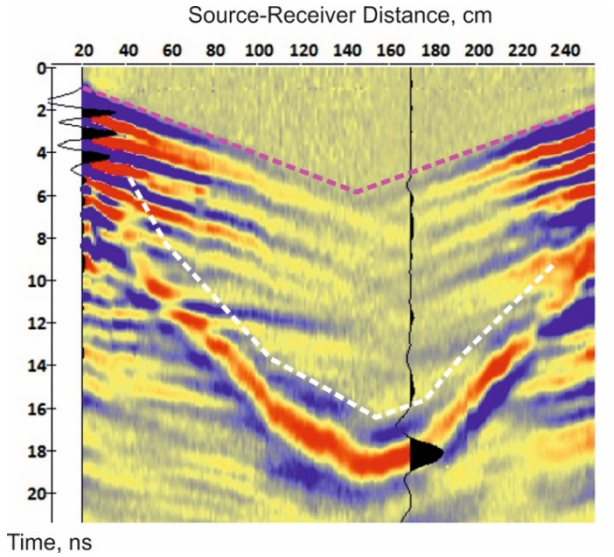

B

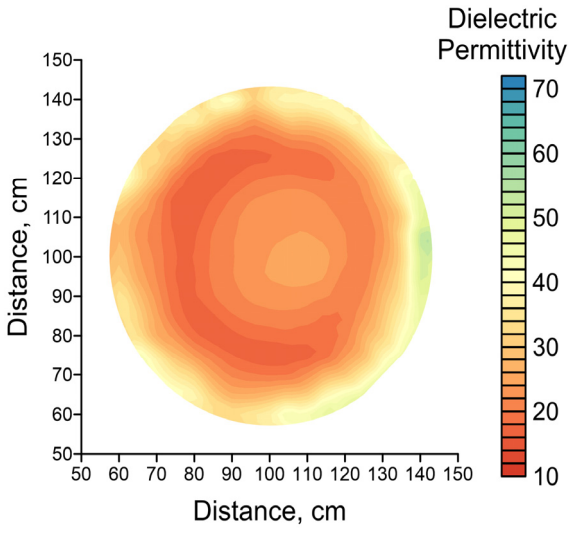

C

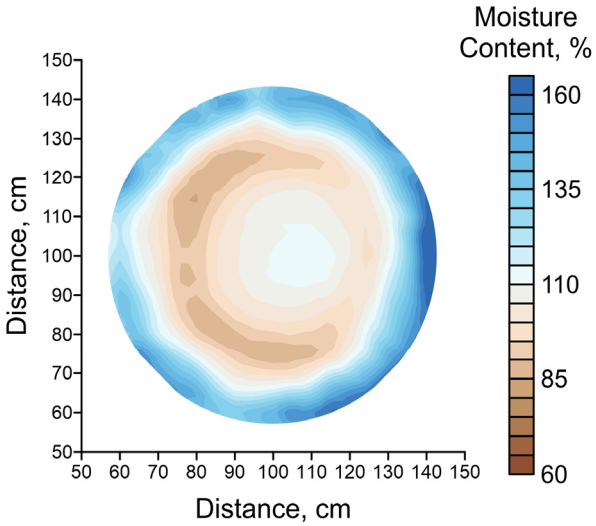

Figure 3. a) Example of Oak trunk GPR tomography data. Purple dotted line: air wave, white dotted line: direct wave; b) dielectric permittivity and moisture content and (c) distribution in the oak trunk.

3.2. Fir tree

In comparison with the data acquired on the oak (Figure 3A), the following features can be distinguished at the data from fir tree (Figure 4A): the direct wave arrival time is lower, and the amplitude is greater. Refracted multiples are not observed. This wave pattern indicates increased velocity values and reduced attenuation of electromagnetic waves inside the trunk and indirectly denotes that the fir is drier than the oak. This conclusion is also endorsed by the result of tomographic inversion (Figure 3A): the average dielectric permittivity is lower (11 with standard

deviation 2, 7) than in live oak (18), and low-permittivity (less than 10) areas are detected. The structure of the trunk is heterogeneous, the structural layers are not so clearly distinguished, but the core, sapwood, bark could be still distinguished.

3.3. European aspen

The radargrams acquired on aspen (Figure 5A) are characterized by a low signal-to-noise ratio compared to the previous data. The amplitude of the direct arrival is lower, and hardly detected against the background of refracted multiple arrivals. Diffraction is observed in the center of the record.

The graph of resistance to drilling (penetrometer record) is co-rendered with the result of GPR tomography. A zone with zero resistance is observed. According to the results of resistography, this zone is defined as a zone of decay. This zone is exactly the same as the area with moisture content is 160% or higher. It is outlined with a thin brown line. This area can be considered to be an area of rot identified using GPR tomography, and confirmed by resistograph. In the South-Western part of the section at the border of this area, a large moisture gradient is observed, which indicates a fundamental change in the properties and structure on this side. It can be concluded that the boundary of the rotten area, with high moisture content not typical to live tree, coincides with the boundary of high gradient zone.

3.4. Chestnut

The data acquired on chestnut are also characterized by a low signal-to-noise ratio, as well as on aspen (Figures 6A and 7A). The wave travelling through the trunk of a chestnut tree (shown in white) is not as distinct as in the case of fir and oak. The dielectric permittivity and moisture content sections demonstrate a zone of increased values with an increased gradient on the boundary, corresponding to water and humus-filled cavity. The shape and size of the cavity at a height of 150 cm are approximately known from visual inspection. They coincide with the area that is highlighted in the moisture section according to previously mentionned characteristics: high moisture content and a high gradient at the boundary. In case of a section at height of 150 cm, the boundary of the rotten area coincides with the contour of moisture value of 143%. The size of the cavity is about 50% of the cross-section area.

In accordance with the same criteria, the boundary of the rotten area is also drawn along the contour line of 143% on the section at height of 95 cm. The rotten area dimensions decrease with depth, and the moisture content inside increases. At the same time, in the south-southwestern part of the section, it is observed at the surface of the trunk. This seems to be a calculation error, most likely due to insufficient accuracy of the trunk geometry or a failure to take into account its three-dimensional structure.

Table 2 shows the moisture content obtained for different trees: average, minimum and maximum values are presented. Similar moisture content values are given in other papers. For example, MC of sound wood is about 100% [24] while for decayed wood it ranges from 100 to 400%.

A

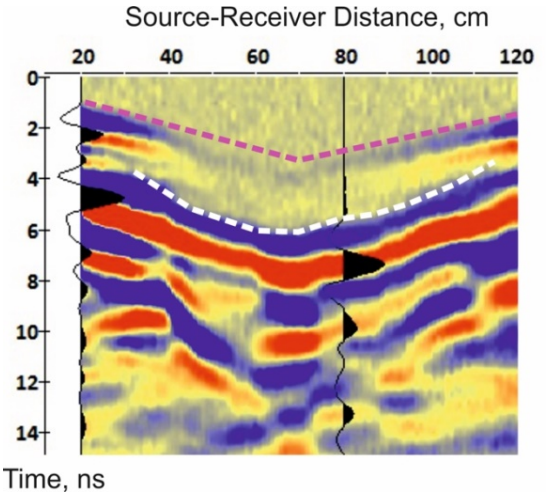

B

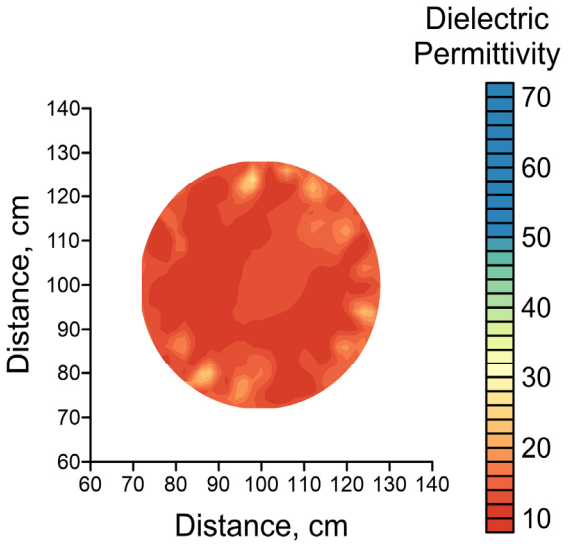

C

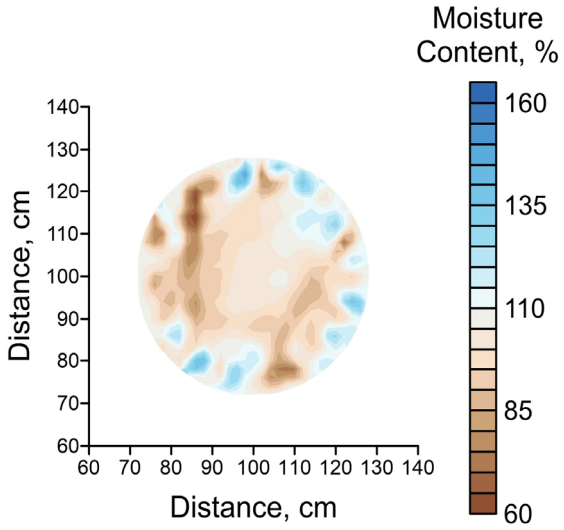

Figure 4. a) Example of fir trunk GPR tomography data. Purple dotted line—air wave; white dotted line—direct wave; b) dielectric permittivity and moisture content and c) distribution in the fir tree trunk.

A

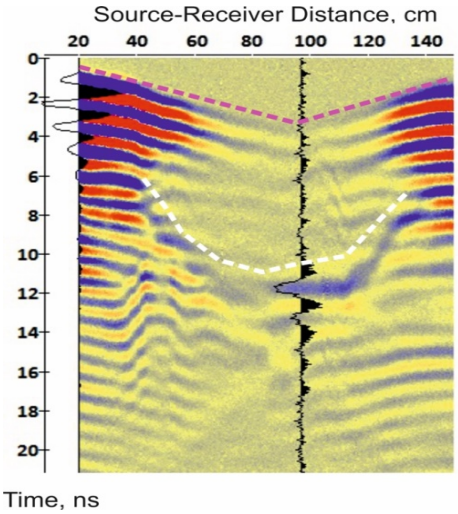

B C

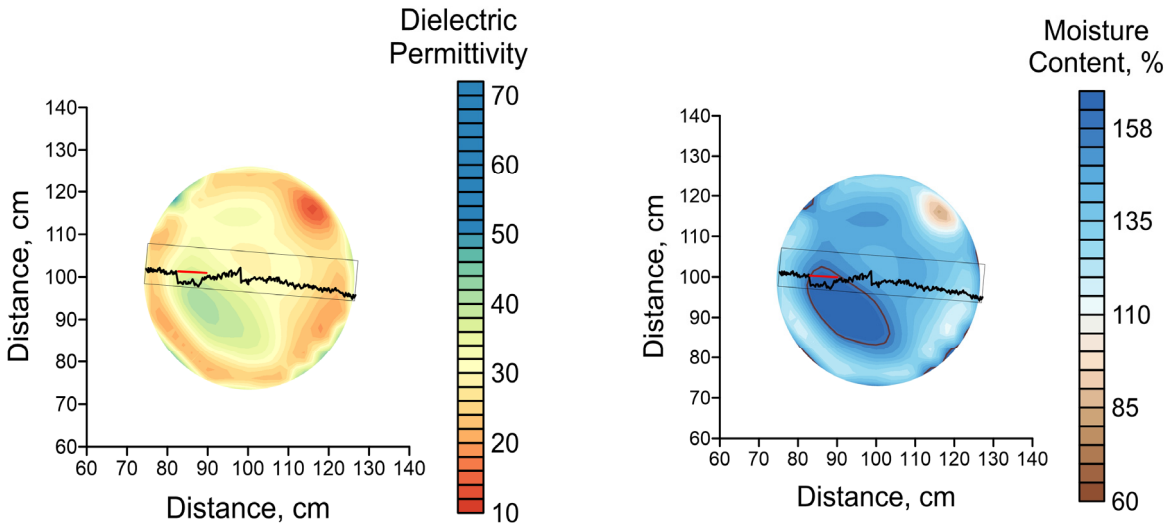

Figure 5. a) Example of Aspen trunk GPR tomography data. Purple dotted line—air wave, white dotted line—direct wave; b) dielectric permittivity and moisture content; (c) distribution in the Aspen trunk. Black line shows penetrometer graph superimposed with the GPR tomography results. Red line shows decayed area. The decayed area is outlined in brown.

A

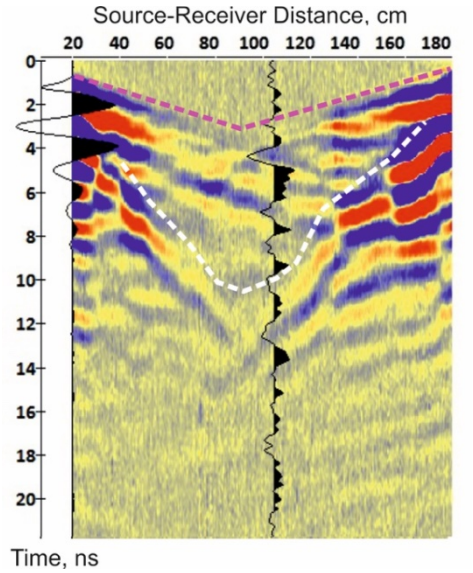

B C

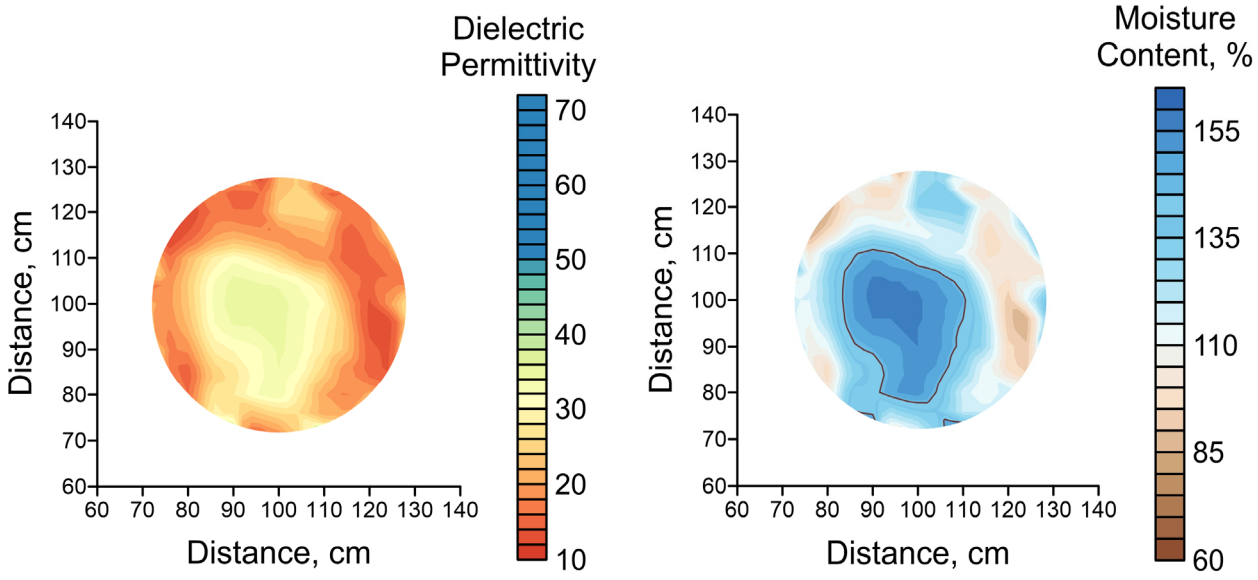

Figure 6. a) Example of Chestnut trunk GPR tomography data obtained at height 150 cm. Purple dotted line—air wave, white dotted line—direct wave, b) dielectric permittivity and moisture content and (c) distribution in the Chestnut trunk. The decayed area is outlined in brown.

A

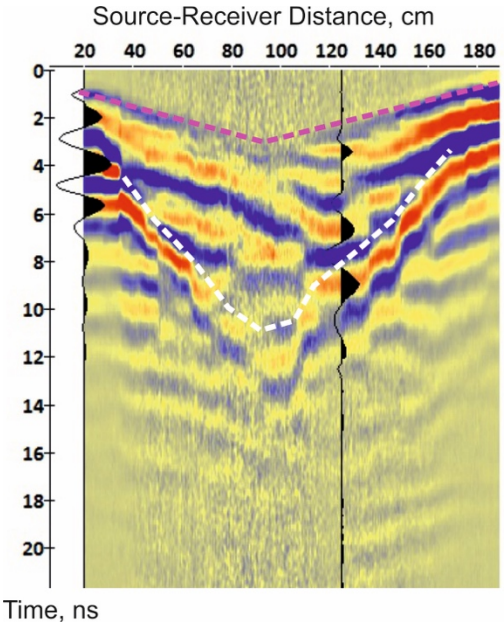

B C

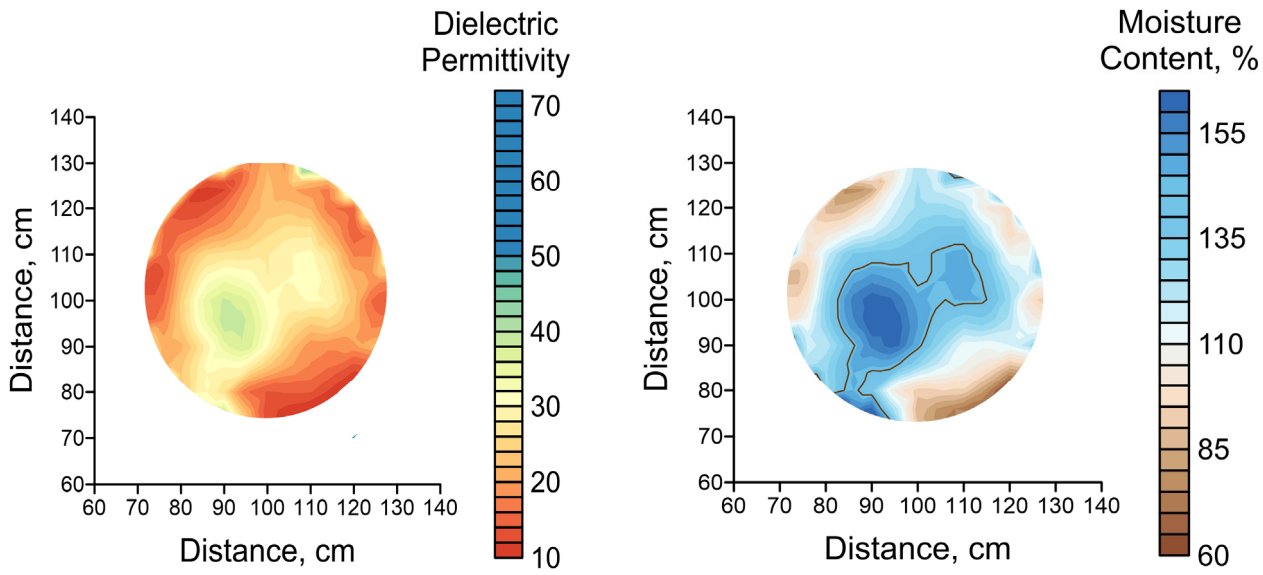

Figure 7. a) Example of Chestnut trunk GPR tomography data obtained at height 95 cm. Purple dotted line—air wave, white dotted line—direct wave, b) dielectric permittivity and moisture content and (c) distribution in the Chestnut trunk. The decayed area is outlined in brown.

Table 2. Moisture content in sections of investigated trees according to the GPR tomography.

Tree specie	Moisture content, %		
	Average ± standard deviation	Max	Min
English oak (Quercus robur)	116 ± 22	174	83
Siberian fir (Picea obovata)	97 ± 11	150	61
European Aspen (Populus tremula)	160 ± 38	224	72
Horse chestnut 150 cm (Castanea dentata)	127 ± 20	224	78
Horse chestnut 95 cm (Castanea dentata)	136 ± 33	224	78

4. Discussion

The GPR mode allows users to select the distance between observation points arbitrarily small, which is especially important in tomographic technique, when accuracy of the solution depends on ray coverage of the area under study. The acquisition geometry, with the source and receivers points located along the perimeter, and not just on two or three sides, ensures uniform ray coverage of the entire section of the trunk. Therefore, a positive result of delineation of the trunk internal structure which matches the results of resistography was expected.

On the other hand, to solve the problem of detection of the rotten area in the trunk, a full cycle of observations and tomographic inversion may not be necessary. A single observation cycle is sufficient to draw the conclusions. In a healthy tree, the direct wave amplitude is consistently high, with an apparent velocity of about 7 cm/ns. The data are characterized by good quality. In a dry tree, good quality data may also be acquired, the amplitude of direct arrival is much higher than the amplitude of air wave, and the apparent velocity ranges from 10 cm/ns. For example, in a tree with wet rot inside, the quality of data deteriorates, the signal-to-noise ratio is close to 1. From the point of view of the electromagnetic wave theory, this can be explained by reflection losses at the boundary of the rotten zone, and scattering due to inhomogeneous structure, and conduction currents due to high moisture content.

In other words, poor data quality is the first criteria of decay in the trunk. In addition to this feature, we identified other features that can be used to detect rot in the trunk: moisture content greater than 140% and increased gradient, which indicates a fundamental change in the structure at the boundary of healthy wood.

A relatively broad range of moisture boundary values is obtained because the moisture content estimate based on correlation relationships is approximate and needs to be calibrated. Moreover, the moisture inside the tree reacts not only to its health condition, but also to weather, shade in the vicinity of a tree and other external and internal factors, affecting the result. Therefore, high moisture content alone is not enough to determine the size of the rot. The range of moisture content calculated for different types of trees corroborates this conclusion (Table 1).

GPR tomography is interesting and promising in moisture content monitoring in healthy trees and estimation of dimensions of physiological parts of the trunk. As we demonstrated, healthy trunk is characterized by circular outlines (presumably the core) and rings (presumably sapwood and bark), which differ not only in moisture content, but also in its gradient. The potential of the technique is associated with increasing the number of observation points and building three-dimensional models of trunks.

It is difficult to draw any conclusions on the dry fir tree and give interpretation of the structure without additional information. To calibrate the GPR method, measurements must be carried out on trees which are supposed to be cut down. The obtained values of dielectric permittivity and moisture content do not contradict the data on dielectric properties: the average, minimum and maximum moisture content obtained for fir is the smallest.

Possible errors in determining the dielectric permittivity and moisture content in trunks are related to velocity estimation and assumptions about the cylindrical structure of a trunk. To obtain a more accurate result, a detailed evaluation of tree trunk geometry is needed. Unfortunately, the authors of the paper had no such opportunity.

In conclusion of the discussion, we have to note that, in comparison with more frequently used common-offset GPR, tomography is a much more labour-intensive method. In order to apply it commercially, some hardware modifications as well as specialized software are required.

5. Conclusions

GPR tomography was used to determine the distribution of dielectric permittivity in the trunk, which is directly related to the moisture of wood. Different parts of the trunk (bark, core, sapwood), as well as healthy and affected areas differ in moisture content, so the method of GPR tomography allowed to see both the structure of the trunk of a healthy tree, and the presence and dimensions of defects. The method has been tested on a small number of trees, therefore our general recommendation is to expand a database of dielectric permittivity vs moisture of tree trunks at a range of densities and temperatures.

Conflict of interest

All authors declare no conflicts of interest in this paper.

References

1. Johnstone D, Moore G, Tausz M, et al. (2010) The measurement of wood decay in landscape trees. *Arboric Urban For* 36: 121–127.
2. Sambuelli L, Socco LV, Godio A, et al. (2003) Ultrasonic, electric and radar measurements for living trees assessment. *B Geofis Teor Appl* 44: 253–279.
3. Rabe C, Ferner D, Fink S, et al. (2004) Detection of decay in trees with stress waves and interpretation of acoustic tomograms. *Arboricultural J* 28: 3–19.
4. Göcke L, Rust S, Weihs U, et al. (2007) Combining sonic and electrical impedance tomography for the non-destructive testing of trees. *Proceedings of 15th international symposium on nondestructive testing of wood. Forest products society*. Madison, 31–42.
5. Leong EC, Burcham DC, Yok-King F (2012) A purposeful classification of tree decay detection tools. *Arboricultural J Int J Urban For* 34: 91–115.
6. Mattheck CG, Breloer H (1994) Field guide for visual tree assessment (VTA). *Arboricultural J Int J Urban For* 18: 1–23.
7. Hayes E (2001) Evaluating Tree Defects, *Safe trees,* 2 Eds., Rochester, 34.

8. Luley CL (2005) *Wood decay fungi common to living urban trees in the Northeast and Central United States*, Naples: Urban Forestry, 61.
9. Rinn F, Schweingruber FH, Schiir E (1996) RESISTOGRAPH and X-ray density charts of wood comparative evaluation of drill resistance profiles and X-ray density charts of different wood species. *Holzforschung* 50: 303–311.
10. Martin T, Günther T (2013) Complex Resistivity Tomography (CRT) for fungus detection on standing oak trees. *Eur J For Res* 132 : 765–776.
11. Gilbert EA, Smiley ET (2004) Picus sonic tomography for the quantification of decay in white oak (Quercus alba) and hickory (Carya spp.). *J Arboric* 30: 277–280.
12. Wessoly L (1995) Fracture diagnosis of trees. Part 3: Boring is no way for reliable fracture diagnosis. *Stadt Und Grün* 9: 635–640.
13. Hagrey SA (2007) Geophysical imaging of root-zone, trunk, and moisture heterogeneity. *J Exp Bot* 58: 839–854.
14. Bassuk N, Grabosky J, Mucciardi A, et al. (2011) Ground-penetrating radar accurately locates tree roots in two soil media under pavement. *Arboric Urban For* 37: 160–166.
15. Zhu SP, Huang CL, Su Y, et al. (2014) 3D Ground penetrating radar to detect tree roots and estimate root biomass in the field. *Remote Sens* 6: 5754–5773.
16. Satriani A, Loperte A, Proto M, et al. (2010) Building damage caused by tree roots: laboratory experiments of GPR and ERT surveys. *Adv Geosci* 24: 133–137.
17. Lorenzo H, Pérez-Gracia V, Novo A, et al. (2010) Forestry applications of ground-penetrating radar. *For Syst* 19: 5–17.
18. Muller W (2003) Timber girder inspection using ground penetrating radar. *OR Insight* 45: 809–812.
19. Pyakurel S (2009) 2D and 3D GPR imaging of wood and fiber reinforced polymer composites. *West Virginia University*, Morgantown
20. Halabe UB, Agrawal S, Gopalakrishnan B (2009) Non-destructive evaluation of wooden logs using ground penetrating radar. *Nondestr Test Eval* 24: 329–346.
21. Colla C (2010) GPR of a timber structural element. *Proceedings of 13th international conference on ground penetrating radar,* Lecce.
22. Rodriguez-Abad I, et al. (2010) Non-destructive methodologies for the evaluation of moisture content in sawn timber structures: ground-penetrating radar and ultrasound techniques. *Near Surf Geophys* 8: 475–482.
23. Jezova J, Lambot S (2019) Influence of bark surface roughness on tree trunk radar inspection. *Ground Penetrating Radar* 2: 1–25. Available from: https://doi.org/10.26376/GPR2019001.
24. Nicolotti G, Socco LV, Martinis R, et al. (2003) Application and comparison of three tomographic techniques for detection of decay in trees. *J Arboric* 29: 66–78.
25. Sudakova MS, Kalashnikov AU, Terentieva EB (2017) GPR tomography as applied to delineation of voids. *Construction Unique Build Struct* 60: 57.
26. Sihvola A (2000) Mixing rules with complex dielectric coefficients. *Subsurf Sens Technol Appl* 1: 393–415.
27. Huisman JA, Hubbard SS, Redman JD, et al. (2003) Measuring soil water content with ground penetrating radar: a review. *Vadose Zone J* 2: 476–491.
28. Hartley I, Hamza MF (2016) Wood: Moisture Content, Hygroscopicity, and Sorption. In: Saleem Hashmi (Editor in chief), *Reference Module in Materials Science and Materials Engineering*, Oxford: Elsevier.

29. Torgovnikov G (1993) *Dielectric properties of wood and wood-based materials*. Berlin, Heidelberg, New-York: Springer-Verlag, 196.
30. Sahin H, Ay N (2004) Dielectric properties of hardwood species at microwave frequencies. *J Wood Sci* 50: 375–380.
31. Sbartaï, ZM, Lataste JF (2008) Evaluation non-destructive de l'humidité du bois par mesures radar et résistivité électrique. *Rapport interne,* Université bordeaux 1, US2B, Ghymac.
32. Jol HM (2009) *Ground penetrating radar theory and applications*, Oxford: Elsevier, 523.
33. Kabir MF, Khalid KB, Daud WM, et al. (1997) Dielectric properties of rubber wood at microwave frequencies measured with an open-ended coaxial line. *Wood Fiber Sci* 29: 319–324.
34. Afzal MT, Colpits B, Galik K (2003) Dielectric Properties of Softwood Species Measured with an Open-ended Coaxial Probe. *In proceedings 8th International IUFRO Wood Drying Conference*, Brasvo, Romania, August, 24–29, 2003; 110–115.
35. Koubaa A, Perré P, Hutcheon RM, et al. (2008) Complex Dielectric Properties of the Sapwood of Aspen, White Birch, Yellow Birch, and Sugar Maple. *Drying Technol* 26: 568–578.
36. Topp GC, Davis JL, Annan AP (1980) Electromagnetic determination of soil water content: measurements in coaxial transmission lines. *Water Resour Res* 16: 574–582.
37. Lin G, Lv JX, Wen J (2014) Research on the relationship between moisture content and the dielectric constant of the tree trunk by the radar wave. *Comput Modell New Technol* 18: 1171–1175.
38. Razafindratsima S, Sbartaï ZM, Demontoux F (2017) Permittivity measurement of wood material over a wide range of moisture content. *Wood Sci Technol* 51: 1421–1431.
39. Acuna L, Basterra LA, Casado M, et al. (2011) Application of resistograph to obtain the density and to differentiate wood species. *Mater Construcc* 61: 451–464.

AIMS Press